4. Strength and Ductility of Reinforced Concrete Members

4.1 Strength and Ductility

It is important to have enough strength and deformation capacities of structural members to assure seismic performance of bridges. This is one of the most important requirements which distinguish the modern seismic design practice from the old generation practice. This importance was widely accepted after the 1971 San Fernando, USA, earthquake. Extensive studies have been conducted for enhancing ductility capacity of reinforced concrete piers and columns. Effect of lateral confinement of concrete, hysteretic behavior of reinforce concrete columns, and various researches for the enhancement of ductility capacity of bridge piers are presented in this chapter.

4.2 Lateral Confinement of Concrete by Ties

1) Lateral Confinement Effect

Reinforced concrete bridge columns exhibit extensive inelastic behavior under a strong seismic disturbance. It is known that the lateral confinement by hoops enhance the ductility and energy dissipation capacities of reinforced concrete columns. Various studies have been conducted for the lateral confinement effects of reinforced concrete columns. Early studies showed that the strength and corresponding longitudinal strain at the strength of concrete confined by a hydrostatic fluid pressure can be represented by

$$f'_{cc} = f'_{c0} + k_1 f_l \tag{4.1}$$

$$\varepsilon_{cc} = \varepsilon_{c0}\left(1 + k_2 \frac{f_l}{f'_{c0}}\right) \tag{4.2}$$

where f'_{cc} and ε_{cc}: the maximum concrete stress and the corresponding strain, respectively, under the lateral fluid pressure f_l, f'_{c0} and ε_{c0}: unconfined concrete strength and corresponding strain, respectively, and k_1 and k_2: coefficients that are function of the concrete mix and the lateral pressure.

Richard et al (1928) found that the averaged value of the coefficients k_1 is equal to 4.1 and $k_2 = 5k_1$ (after Mander, Priestley and Park 1986).

To represent the confinement effect, it is necessary to define an equation for the ascending branch and the descending branch, the peak strength and corresponding strain f_{cc} and ε_{cc}, respectively, and the stress and strain at the ultimate f_{cu} and ε_{cu}, respectively. Kent and Park (1971) developed a stress-strain model consisting of a second-order parabola ascending branch and a straight descending branch. The effect of lateral confinement is accounted for by varying the slope of the descending branch. in this mode. After the 1971 San Fernando earthquake, the importance of enhancing the ductility capacity became well known. The model developed by Kent and Park triggered the research on the confinement effect. Park et al (1982) revised this model so that the enhancement of concrete strength was included in this model. The confinement effect was represented to be proportional to the volumetric ratio and yield strength of hoops.

Mander, Priestley and Park (1988) developed an empirical equation to represent the confinement effect for both circular and rectangular sections as

$$f_c = \frac{f'_{cc} x r}{r - 1 + x'} \tag{4.3}$$

where,

$$x = \frac{\varepsilon_c}{\varepsilon_{cc}} \tag{4.4}$$

$$\varepsilon_{cc} = \varepsilon_{c0} \left\{ 1 + 5 \left(\frac{f'_{cc}}{f'_{c0}} - 1 \right) \right\} \tag{4.5}$$

$$r = \frac{E_c}{E_c - E_{\text{sec}}} \tag{4.6}$$

$$E_c = 5{,}000 \sqrt{f'_{c0}} \tag{4.7}$$

$$E_{\text{sec}} = \frac{f'_{cc}}{\varepsilon_{cc}} \tag{4.8}$$

where f'_{cc}: compressive strength of concrete, ε_c: longitudinal compressive concrete strain, f'_{c0} and ε_{c0}: the unconfined concrete strength and corresponding strain, respectively, E_c: tangential modulus of elasticity of the concrete (MPa).

Mander, Priestley and Park (1988) also developed unloading and reloading paths.

Hoshikuma, Kawashima, Nagaya and Taylor (1997) developed an empirical model for the lateral confinement based on uniaxial loading test for circular and square cylinders with a diameter or width of 200 mm and 500 mm and height of 600 mm, and a diameter or width of 500 mm and a height of 1,500 mm. They assume that the concrete stress in the ascending branch is represented as

$$f_c = C_1 {\varepsilon_c}^n + C_2 \varepsilon_c + C_3 \tag{4.9}$$

where parameters C_1, C_2, C_3 and n are determined from the following boundary conditions.

$$f_c = 0 \quad \text{at} \quad \varepsilon_c = 0 \tag{4.10}$$

$$\frac{df_c}{d\varepsilon_c} = E_c \quad \text{at} \quad \varepsilon_c = 0 \tag{4.11}$$

$$f_c = f_{cc} \quad \text{at} \quad \varepsilon_c = \varepsilon_{cc} \tag{4.12}$$

$$\frac{df_c}{d\varepsilon_c} = 0 \quad \text{at} \quad \varepsilon_c = \varepsilon_{cc} \tag{4.13}$$

where f_{cc} and ε_{cc}: compressive strength of concrete and corresponding strain, respectively. By representing the descending branch by a straight line, one obtains

$$f_c = \begin{cases} E_c \varepsilon_c \left\{ 1 - \dfrac{1}{n} \left(\dfrac{\varepsilon_c}{\varepsilon_{cc}} \right)^{n-1} \right\} & 0 < \varepsilon_c \le \varepsilon_{cc} \\ f_{cc} - E_{des} (\varepsilon_c - \varepsilon_{cc}) & \varepsilon_{cc} < \varepsilon_c < \varepsilon_{cu} \end{cases} \tag{4.14}$$

where,

$$n = \frac{E_c \varepsilon_{cc}}{E_c \varepsilon_{cc} - f_{cc}} \tag{4.15}$$

$$\varepsilon_{cu} = \varepsilon_{cc} + \frac{f_{cc}}{2E_{des}} \tag{4.16}$$

where E_{des} : deterioration rate at the descending branch and ε_{cu} : ultimate strain of concrete.

The compressive stress of concrete and corresponding strain f_{cc} and ε_{cc} and the deteriorating rate of the descending branch E_{des} are given as

$$\frac{f_{cc}}{f_{c0}} = 1 + 3.8\alpha \frac{\rho_s f_{yh}}{f_{c0}} \tag{4.17}$$

$$\varepsilon_{cc} = 0.002 + 0.033\beta \frac{\rho_s f_{yh}}{f_{c0}} \tag{4.18}$$

$$E_{des} = 11.2 \frac{f_{co}{}^2}{\rho_s f_{yh}} \tag{4.19}$$

$$\rho_s = \frac{4A_h}{s \cdot d} \tag{4.20}$$

where α and β are shape coefficients, and are 1.0 and 1.0, respectively, for circular sections, and 0.2 and 0.4, respectively, for square sections, and ρ_s : volumetric hoop reinforcement ratio, A_h , f_{yh} and s : sectional area, yield strength and interval of hoops, respectively, and d : width of a column.

Fig. 4.1 shows the confinement effect of concrete between the experimental and empirical results for the circular and square cylinders with a diameter or width of 200 mm and 500mm. The empirical formulae represent a good agreement with the experimental results.

Sakai and Kawashima (2000) developed unloading and reloading paths for (1) full unloading and full reloading, (2) partial unloading and full reloading, and (3) full unloading and partial unloading. Effect of repeating unloading and reloading is also included in the model.

a) Hysteresis for repeated full unloading and reloading

If a full unloading occurs from a skeleton curve at stress $f_{ul,1}$ and strain ε_{ul} as shown in Fig. 4.2, this unloading path intersects the zero stress axis at a plastic strain $\varepsilon_{pl,1}$. If a full reloading occurs at this strain, the reloading path reaches a stress $f_{ul,2}$ at the unloading strain ε_{ul}. If a full unloading and a full reloading repeat n times (n=1,2,….), the plastic strain $\varepsilon_{pl,n}$ increases and the reloaded stress $f_{ul,n}$ at the unload strain ε_{ul} decreases. By defining the normalized stress $\tilde{f}$, the normalized strain $\tilde{\varepsilon}$, the stress deterioration rate β_n , and the increasing rate of plastic strain γ_n as

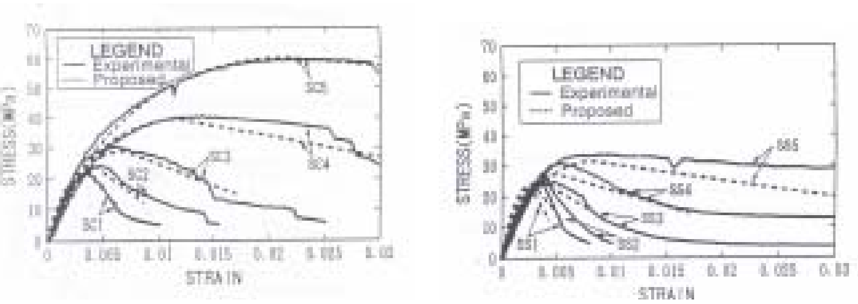

(a) 600 mm tall circular cylinders (ϕ200mm) (b) 1,500 mm tall circular cylinders(ϕ500 mm)

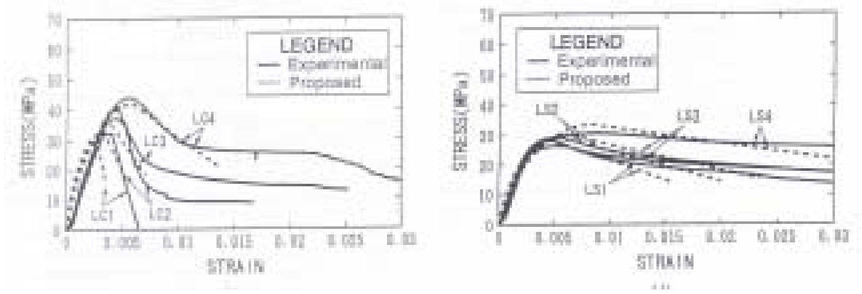

(a) 600 mm tall square cylinders (width=200mm) (b) 1,500 mm tall circular cylinders (width=500 mm)

Fig.4.1 Comparison of Confinement Effect between Empirical and Experimental

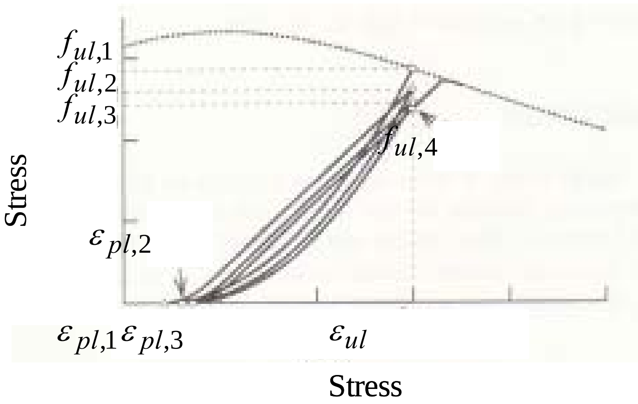

Fig.4.2 Plastic Strain $\varepsilon_{pl,n}$ and Reload Stress $f_{ul,n}$ when Unloading occurs at ε_{ul}

$$\tilde{f} = \frac{f_c}{f_{ul,n}} \tag{4.21}$$

$$\tilde{\varepsilon} = \frac{\varepsilon_c - \varepsilon_{pl,n}}{\varepsilon_{ul} - \varepsilon_{pl,n}} \tag{4.22}$$

$$\beta_n = \frac{f_{ul,n+1}}{f_{ul,n}} \tag{4.23}$$

$$\gamma_n = \frac{\varepsilon_{ul} - \varepsilon_{pl,n}}{\varepsilon_{ul} - \varepsilon_{pl,n-1}} \tag{4.24}$$

full unloading and full reloading paths are represented as

Unloading

$$f_c = f_{ul,n}\left(\frac{\varepsilon_c - \varepsilon_{pl,n}}{\varepsilon_{ul} - \varepsilon_{pl,n}}\right)^2 \tag{4.25}$$

<u>Reloading</u>

$$f_c = \begin{cases} 2.5 f_{ul,n}\left(\dfrac{\varepsilon_c - \varepsilon_{pl,n}}{\varepsilon_{ul} - \varepsilon_{pl,n}}\right)^2 & 0 \le \tilde{\varepsilon} < 0.2 \\ f_{ul,n+1} + E_{rl}(\varepsilon_c - \varepsilon_{ul}) & 0.2 \le \tilde{\varepsilon} \le 1.0 \end{cases} \tag{4.26}$$

where

$$E_{rt} = \frac{f_{ul,n+1} - 0.1 f_{ul,n}}{0.8 \times (\varepsilon_{ul} - \varepsilon_{pl,n})} \tag{4.27}$$

$$\varepsilon_{pl,1} = \begin{cases} 0 & 0 \le \varepsilon_{ul} \le 0.001 \\ 0.4(\varepsilon_{ul} - 0.001) & 0.001 < \varepsilon_{ul} < 0.0035 \\ 0.96(\varepsilon_{ul} - 0.00245) & 0.0035 \le \varepsilon_{ul} \le 0.03 \end{cases} \tag{4.28}$$

<u>*n*=1 and 2</u>

$$\beta_n = \begin{cases} 1 & 0 \le \varepsilon_{ul} \le 0.001 \\ 1 - (10n + 22)(\varepsilon_{ul} - 0.001) & 0.001 < \varepsilon_{ul} < 0.0035 \\ 0.92 + 0.025(\mathrm{n} - 1) & 0.0035 \ge \varepsilon_{ul} \le 0.03 \end{cases} \tag{4.29}$$

<u>n larger than or equal to 3</u>

$$\beta_n = \begin{cases} 1 & 0 \le \varepsilon_{ul} \le 0.001 \\ 1 - (2n + 8)(\varepsilon_{ul} - 0.001) & 0.001 < \varepsilon_{ul} < 0.0035 \\ 0.965 + 0.005(n - 3) & 0.0035 \le \varepsilon_{ul} < 0.03 \end{cases} \tag{4.30}$$

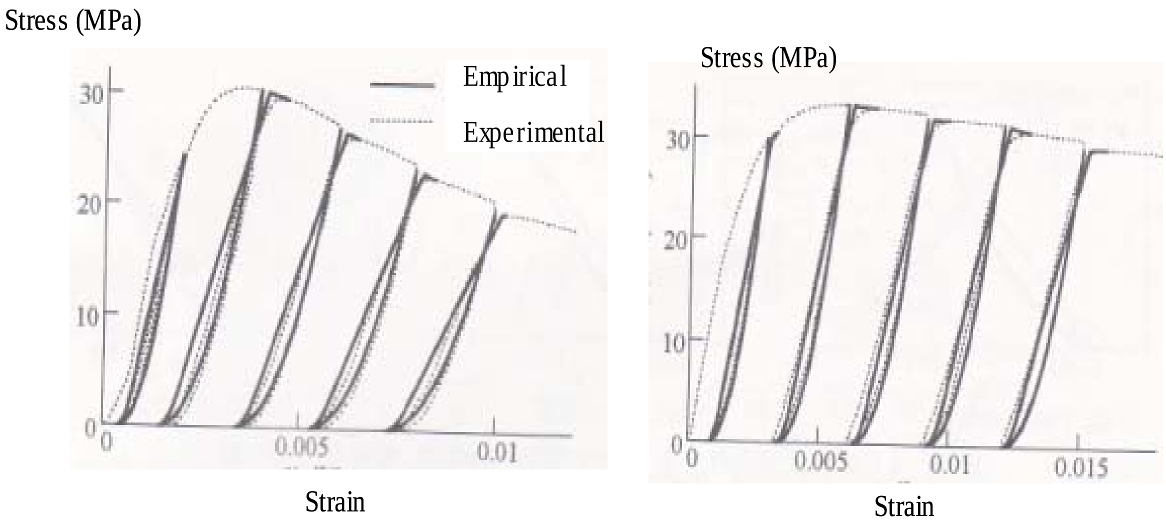

(a) f_{c0}=23.0MPa, $\rho_s = 0.67\%$ (b) f_{c0}=23.0MPa, ρ_s=1.33%

Fig.4.3 Full Unloading and Full Reloading Hystereses Repeated Once

$$\gamma_n = \begin{cases} 0.945 & n = 2 \\ 0.965 + 0.005(n-3) & n \geq 3 \end{cases} \tag{4.31}$$

Fig. 4.3 shows an applicability of Eqs. (4.22)-(4.31) for a full unloading and a full reloading at 5 points on a skeleton curve of the concrete cylinders with the volumetric hoop reinforcement ratio ρ_s of 0.67% and 1.33 %. Fig. 4.4 shows a comparison of hysterese when unloading and reloading are repeated ten times with the unloading strain ε_{ul} of 0.005 for a concrete cylinder with ρ_s of 1.14%. Experimental and empirical paths are compared for 5th and 10th unloading and reloading. From those comparison, it is apparent that Eqs. (4.22)-(4.31) provide a good estimate to the experimental results.

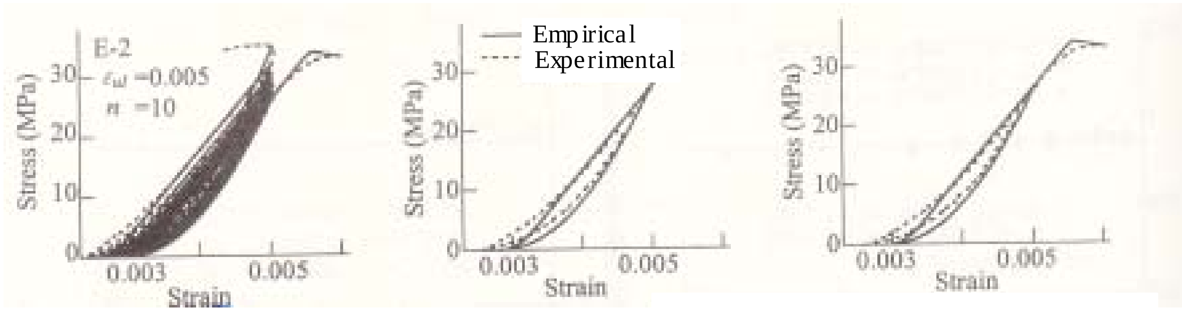

(a) Unloading and Reloading Repeated Ten times

(b) 5th Unloading and Reloading

(c) 10th Unloading and Reloading

Fig.4.4 Full Unloading and Full Reloading Repeated 10 Times with ε_{ul} =0.005

b) Hystereses for partial unloading and full reloading

When a partial unloading occurs at an unloading strain ε_{ul}, a partial unloading path must be the same with the full unloading path as shown in Fig. 4.5. As a result, Eq. (4.25) can still be used for the partial unloading path. To represent the degree of a partial unloading, a parameter is introduced as

$$\beta_{UL} = \frac{f_{rl}}{f_{ul,1}} \tag{4.32}$$

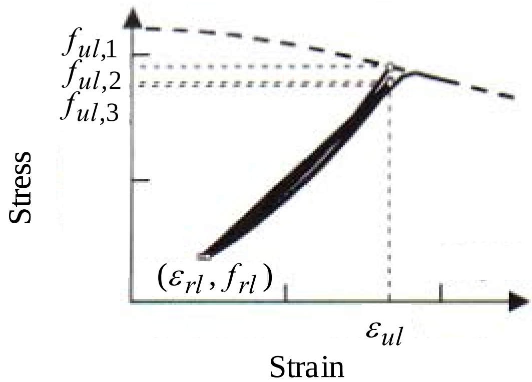

Fig.4.5 Partial Unloading and Full Reloading

When an reloading occurs at a reloading stress f_{rl} and a corresponding reloading strain ε_{rl}, a full reloading path from this point is represented as

$$f_c = E_{prl}(\varepsilon_c - \varepsilon_{ul}) + f_{ul,n+1} \tag{4.33}$$

where

$$E_{prl} = \frac{f_{ul,n+1} - f_{rl}}{\varepsilon_{ul} - \varepsilon_{rl}} \tag{4.34}$$

The stress $f_{ul,n+1}$ can be determined by Eqs. (4.29) and (4.30).

c) Hystereses for full unloading and partial reloading

After a full unloading from ε_{ul} to $\varepsilon_{pl,1}$, when a partial reloading occurs to reach a strain $\varepsilon_{ul,in}$, the hysteresis becomes as shown in Fig. 4.6. By fully unloading from $\varepsilon_{ul,in}$, the strain progresses to $\varepsilon_{pl,2}$. A partial reloading again from $\varepsilon_{pl,2}$ to $\varepsilon_{ul,in}$ results in a reduction of

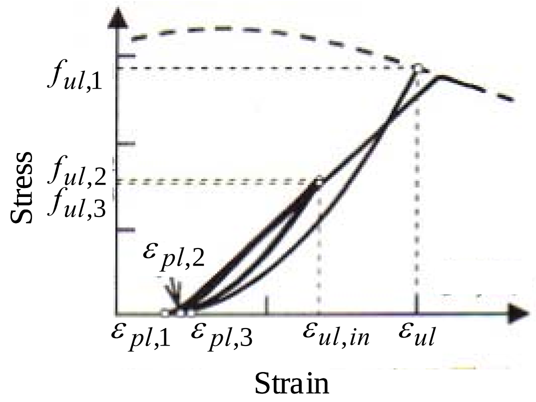

Fig.4.6 Full Unloading and Partial Reloading

corresponding stress to $f_{ul,2}$. Defining the normalized stress $\tilde{f}_{in}$, normalized strain $\tilde{\varepsilon}_{in}$, the stress deterioration rate $\beta_{in,n}$ and the plastic strain increasing rate $\gamma_{in,n}$ as

$$\tilde{f}_{in} = \frac{f_c}{f_{in,n}} \tag{4.35}$$

$$\tilde{\varepsilon}_{in} = \frac{\varepsilon_c - \varepsilon_{pl,n}}{\varepsilon_{ul,in} - \varepsilon_{pl,n}} \tag{4.36}$$

$$\beta_{in,n} = \frac{f_{in,n+1}}{f_{in,n}} \tag{4.37}$$

$$\gamma_{in,n} = \frac{\varepsilon_{ul,in} - \varepsilon_{pl,n}}{\varepsilon_{ul,in} - \varepsilon_{pl,n-1}} \tag{4.38}$$

a full unloading and reloading paths are expressed by

<u>Unloading</u>

$$f_c = f_{in,n}\left(\frac{\varepsilon_c - \varepsilon_{pl,n}}{\varepsilon_{ul} - \varepsilon_{pl,n}}\right)^2 \tag{4.39}$$

Reloading

$$f_c = \begin{cases} 2.5 f_{in,n}\left(\dfrac{\varepsilon_c - \varepsilon_{pl,n}}{\varepsilon_{ul} - \varepsilon_{pl,n}}\right)^2 & 0 \le \tilde{\varepsilon}_{in} < 0.2 \\ f_{in,n+1} + E_{rl,in}(\varepsilon_c - \varepsilon_{ul,in}) & 0.2 \le \tilde{\varepsilon}_{in} \le 1 \end{cases} \tag{4.40}$$

where,

$$E_{rl,in} = \frac{f_{in,n+1} - 0.1 f_{in,n}}{0.8(\varepsilon_{ul,in} - \varepsilon_{pl,n})} \tag{4.41}$$

$$\beta_{in,n} = \beta_n + 0.2(1 - \gamma_{RL}) \tag{4.42}$$

$$\gamma_{in,n} = \gamma_n + 0.2(1 - \gamma_{RL}) \tag{4.43}$$

$$\gamma_{RL} = \frac{\varepsilon_{ul,n} - \varepsilon_{pl,1}}{\varepsilon_{ul} - \varepsilon_{pl,1}} \tag{4.44}$$

Fig. 4.7 shows a comparison of a hysteresis of a full reloading after a partial unloading for a cylinder with ρ_s =1.14%. The unloading occurs at ε_{ul} =0.006 until β_{UL} =0.5. The hystereses for the 1st and the 5th cycles are presented here. Eqs. (4.25) and (4.33) are used to evaluate the empirical hystereses. The empirical results show a good agreement with the test results.

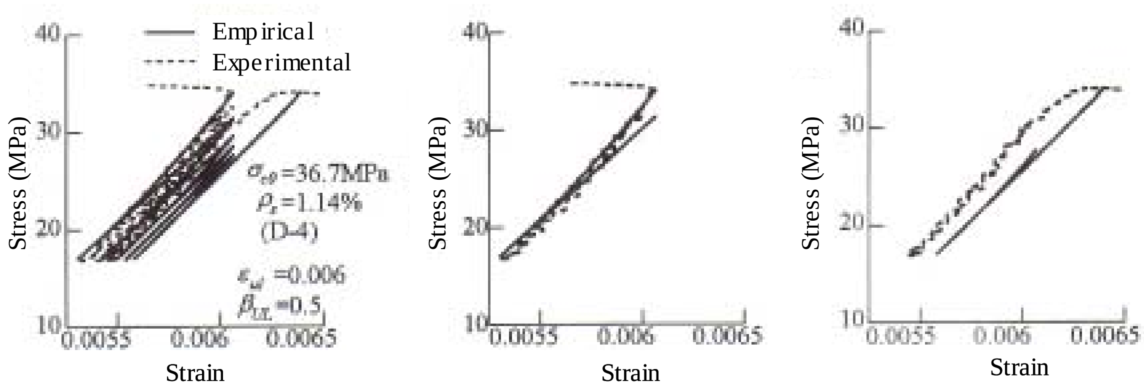

(a) Total Hystereses (b) 1st Cycle (c) 5th Cycle

Fig.4.7 Full Unloading and Partial Reloading Repeated Ten Times

Fig. 4.8 shows a comparison of hystereses of a partial reloading after a full unloading at ε_{ul} equal to 0.005 for a cylinder with ρ_s =1.14%. The reloading occurs until γ_{RL} equal to 0.7. After fully unloaded at ε_{ul}, the reloading and the unloading were repeated two times in this example. The empirical hystereses by Eqs. (4.39) and (4.40) agree well with the experimental results.

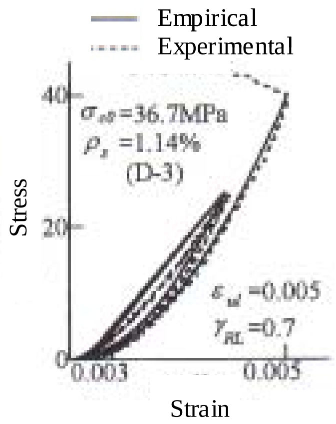

Fig.4.8 Full Unloading and Partial Reloading

2) Lateral Confinement of Concrete by Carbon Fiber Sheets

Carbon fiber sheets are well used for seismic retrofit of existing bridge piers. Lateral confinement effect of concrete by carbon fiber sheets is quite different from the confinement of concrete by hoops. A carbon fiber sheet consists of a number of carbon fiber strings included in a textile. At this moment, carbon fiber sheets having 200 g/m^2 and 300 g/m^2 are available. Their nominal elastic modulus is 230 MPa or 390 MPa and a nominal rupture strain is 1.5%. A carbon fiber sheet is elastic until rupture occurs. Consequently, a carbon fiber sheet has a similar elastic modulus with hoop bars, but has nearly five times larger elastic deformation capacity. In a reinforced concrete column confined by hoops, the confinement force is saturated at the yield of the hoops. On the other hand, in a reinforced concrete column confined by carbon fiber sheets, the confinement force builds up until rupture of the carbon fiber sheet.

Hosotani and Kawashima (1998) develop a constitutive model of concrete confined by carbon fiber sheets, and later they extended this model to include the confinement by both existing hoops and carbon fiber sheets (Hosotani and Kawashima 1999, Kawashima, Hosotani, Yoneda 2000).

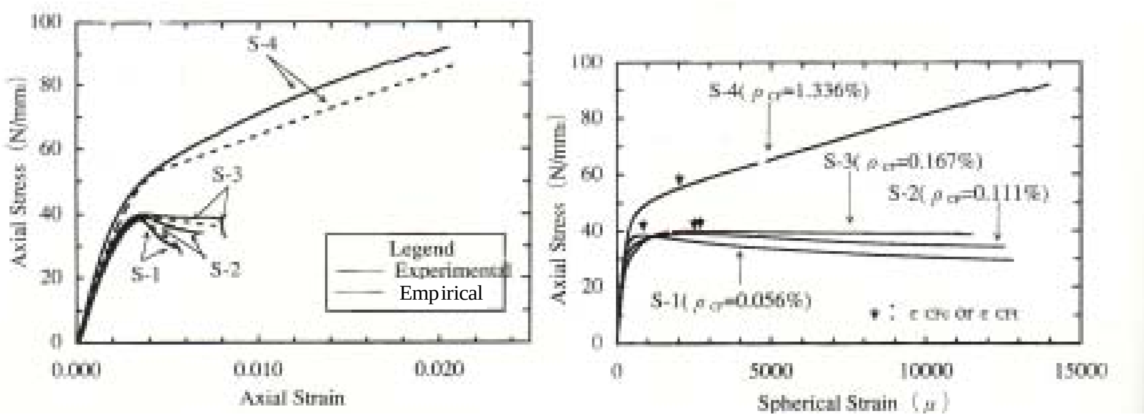

(a) Axial Stress vs. Axial Strain (b) Axial Stress vs. Spherical Strain

Fig.4.9 Stress vs. Strain Relation of Concrete Confined by Carbon Fiber Sheets

Fig. 4.9 shows an example of axial stress f_c vs. axial concrete strain ε_c relation, and axial stress f_c vs. spherical concrete strain relation. To represent an amount of carbon fiber sheets, similar to the volumetric tie reinforcement ratio ρ_s by Eq. (4.20), a carbon fiber sheet ratio (volumetric ratio) ρ_{CF} is defined as

$$\rho_{CF} = \frac{4n \cdot t_{CF}}{d} \qquad (4.45)$$

where t_{CF}: thickness of a CFS (mm), n: number of CFS wrapped, and *d*: diameter of a concrete cylinder (mm). In Fig. 4.9, confined concrete has a peak strength at spherical strains between 1,100 and 2,500 μ if the carbon fiber ratio ρ_{CF} is smaller than 0.167%. One denotes this spherical strain as ε_{CFc}, the stress of CFS corresponding to this ε_{CFc} is between 250 and 550 MPa, which is only 10% of the CFS strength. On the other hand, concrete stress f_c continues to increase in the confined concrete with a larger ρ_{CF} although the stiffness gradually deteriorates from a pre-deterioration value to a post-deterioration value. Defining the spherical strain where the stiffness has shifted to the post-deterioration stiffness as ε_{CFt}, ε_{CFt} is in the range from 1,800 to 1,900 μ. It is known that when the spherical strain of unconfined concrete reaches 1,100-2,500 μ, the concrete starts to suffer damage resulting in the deterioration of stiffness. This spherical strain is in the similar range with ε_{CFc} and ε_{CFt}. This may be because the deterioration of concrete stress at ε_{CFc} or ε_{CFt} result from the deterioration of concrete.

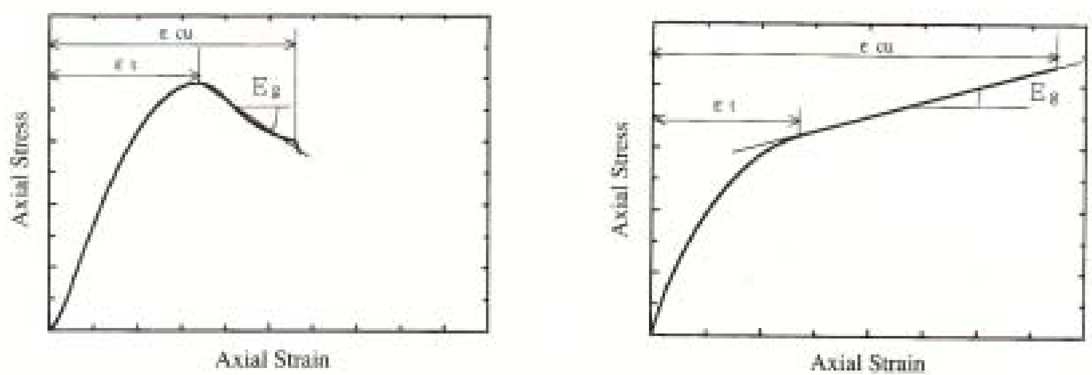

(a) $E_g < 0$ (b) $E_g \geq 0$

Fig.4.10 Stress vs. Strain Relation of Concrete Confined by Carbon Fiber Sheets

a) Lateral Confinement of Concrete by CFS

Depending on the amount of CFS, the stress vs. strain relation takes a form either (a) or (b) in Fig. 4.10. If one denotes the post-deterioration stiffness as E_g, based on experimental test results for circular and square cylinder confined by CFS E_g is evaluated as

Circular sections

$$E_g = -0.658 \frac{{f_{c0}}^2}{\rho_{CF} \varepsilon_{CFt} E_{CF}} + 0.078 \sqrt{\rho_{CF}} E_{CF} \qquad (4.46)$$

Square sections

$$E_g = -1.198 \frac{{f_{c0}}^2}{\rho_{CF}\varepsilon_{CFt}E_{CF}} + 0.012\sqrt{\rho_{CF}}E_{CF} \tag{4.47}$$

where E_{CF} : elastic modulus of CFS. It is noted that E_{des} is positively defined at the descending branch in Eq. (4.18), while it is defined as shown in Fig. 4.10.

When E_g <0, the stress vs. strain relation defined by Eq. (4.14) is used with slight modifications as

$$f_c = \begin{cases} E_c\varepsilon_c\left\{1 - \frac{1}{n}\left(\frac{\varepsilon_c}{\varepsilon_t}\right)^{n-1}\right\} & 0 \le \varepsilon_c \le \varepsilon_t \\ f_t + E_g(\varepsilon_c - \varepsilon_t) & \varepsilon_t \le \varepsilon_c \le \varepsilon_{cu} \end{cases} \tag{4.48}$$

where

$$n = \frac{E_c\varepsilon_t}{E_c\varepsilon_t - f_t} \tag{4.49}$$

where f_t and ε_t represent the concrete stress where the stiffness has shifted to the post-deterioration stiffness and the corresponding strain. When E_g <0, f_t is equal to f_{cc}.

When $E_g \ge 0$, the stress vs. strain relation is expressed as

$$f_c = E_c\varepsilon_c\left\{1 - \frac{1}{n}\left(1 - \frac{E_g}{E_c}\right)\left(\frac{\varepsilon_c}{\varepsilon_t}\right)^{n-1}\right\} \tag{4.50}$$

where

$$n = \frac{(E_c - E_g)\varepsilon_t}{E_c\varepsilon_t - f_t} \tag{4.51}$$

Eq. (4.50) was derived by using Eq. (4.9). Among four boundary conditions by Eqs. (4.10)-(4.13), Eqs. (4.12) and (4.13) were replaced as

$$f_c = f_t \quad \text{at} \quad \varepsilon_c = \varepsilon_t \tag{4.52}$$

$$\frac{df_c}{d\varepsilon_c} = E_g \quad \text{at} \quad \varepsilon_c = \varepsilon_t \tag{4.53}$$

Three parameters are now required to determine the constitutive relation of concrete confined by CFS, i.e., stress f_t and corresponding strain ε_t where the stiffness has shifted to the post-deterioration stiffness, and the ultimate strain ε_{cu}. They are given as

<u>Circular sections</u>

$$\frac{f_t}{f_{c0}} = 1.0 + 1.93\frac{\rho_{CF}\varepsilon_{CFt}E_{CF}}{f_{c0}} \tag{4.54}$$

$$\varepsilon_t = 0.00343 + 0.00939 \frac{\rho_{CF} \varepsilon_{Cf} E_{CF}}{f_{c0}} \tag{4.55}$$

$$\varepsilon_{cu} = 0.00383 + 0.1014 \left(\frac{\rho_{CF} f_{CF}}{f_{c0}} \right)^{\frac{3}{4}} \left(\frac{f_{CF}}{E_{CF}} \right)^{\frac{1}{2}} \tag{4.56}$$

Square sections

$$\frac{f_t}{f_{c0}} = 1.0 + 1.53 \frac{\rho_{CF} \varepsilon_{CF} E_{CF}}{f_{c0}} \tag{4.57}$$

$$\varepsilon_t = 0.00330 + 0.00995 \frac{\rho_{CF} \varepsilon_{CF} E_{CF}}{f_{c0}} \tag{4.58}$$

$$\varepsilon_{cu} = 0.00340 + 0.0802 \left(\frac{\rho_{CF} f_{CF}}{f_{c0}} \right)^{\frac{3}{4}} \left(\frac{f_{CF}}{E_{CF}} \right)^{\frac{1}{2}} \tag{4.59}$$

where f_{CF} represent strength of CFS.

Fig. 4.11 shows comparisons of experimental and empirical relations for concrete cylinders with circular and square sections. They are confined by CFS with CFS strength of 230 MPa or 392 MPa. Empirical stress vs. strain relations agree well with the experimental results.

b) Lateral Confinement of Concrete by both CFS and Ties

Even if the existing ties in a reinforced concrete column are insufficient to confine the core concrete, they must contribute to the confinement as well as CFS if they do not suffer damage during an excitation. Consequently it is interesting to evaluate an interaction of existing ties and CFS. The above empirical formulae are extended to include the effect of existing ties.

The lateral confinement of concrete by Eqs. (4.14)-(4.19) are rewritten using the notations in this section ($\varepsilon_{cc} \to \varepsilon_t$, $f_{cc} \to f_t$, $E_{des} \to -E_g$) as

$$f_c = \begin{cases} E_c \varepsilon_c \left\{ 1 - \dfrac{1}{n} \left(\dfrac{\varepsilon_c}{\varepsilon_t} \right)^{n-1} \right\} & 0 \le \varepsilon_c \le \varepsilon_t \\ f_t + E_g (\varepsilon_c - \varepsilon_t) & \varepsilon_t \le \varepsilon_c \le \varepsilon_{cu} \end{cases} \tag{4.60}$$

where

$$n = \frac{E_c \varepsilon_t}{E_c \varepsilon_t - f_t} \tag{4.61}$$

$$\frac{f_t}{f_{c0}} = \begin{cases} 1.0 + 2.2 \dfrac{\rho_s f_{yh}}{f_{c0}} & \text{circular sections} \\ 1.0 + 0.76 \dfrac{\rho_s f_{yh}}{f_{c0}} & \text{square sections} \end{cases} \tag{4.62}$$

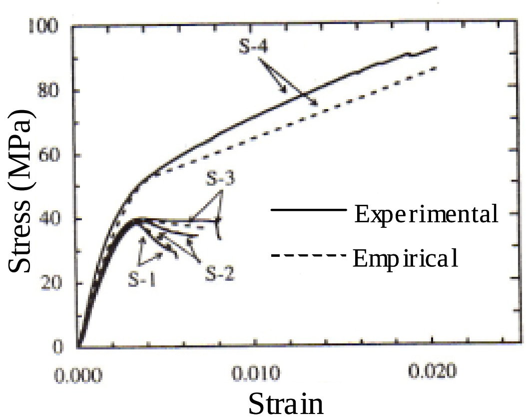

(a) Circular, $f_{CF} = 230MPa$

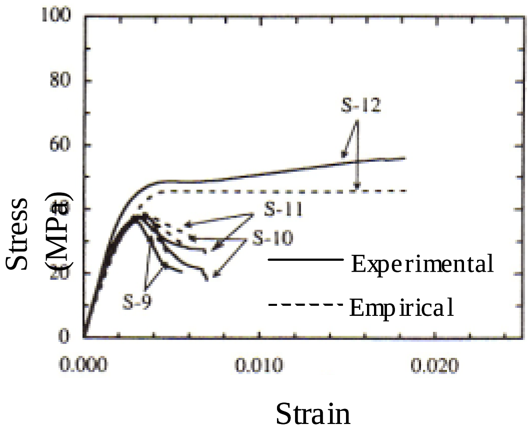

(b) Square, $f_{CF} = 230MPa$

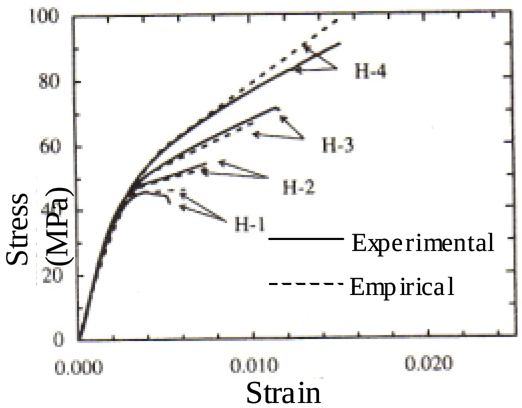

(c) Circular, $f_{CF} = 392MPa$

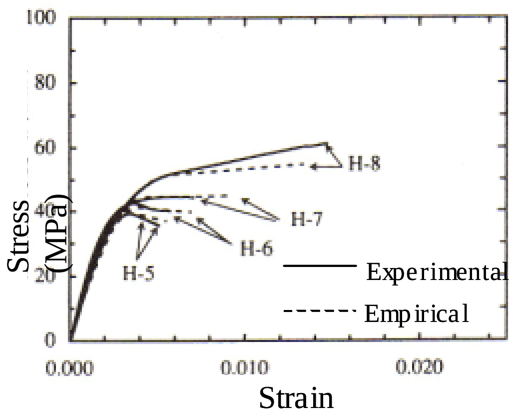

(d) Square, $f_{CF} = 392MPa$

Fig.4.11 Stress vs. Strain Relation of Concrete cylinder Confined by CFS

$$\varepsilon_t = \begin{cases} 0.003 + 0.107 \dfrac{\rho_s f_{yh}}{f_{c0}} & \text{circular sections} \\ 0.003 + 0.0114 \dfrac{\rho_s f_{yh}}{f_{c0}} & \text{square sections} \end{cases} \tag{4.63}$$

$$E_g = -11.2 \frac{{f_{c0}}^2}{\rho_s f_{yh}} \tag{4.64}$$

It is noted here that Eqs. (4.62) and (4.63) are slightly re-evaluated assuming that ε_{c0} is equal to 0.003.

Comparing Eq. (4.54) and Eq. (4.62), one notices a considering similarity. For example, the term of 1.93 $\rho_{CF}\varepsilon_{CF}E_{CF}$ (circular sections) in the right hand side of Eq. (4.54) represents an increasing rate of axial stress f_c at $\varepsilon_c = \varepsilon_t$ by wrapping CFS around the concrete cylinder. Since $\rho_{CF}\varepsilon_{CF}E_{CF}$ represents the confining stress by CFS at the strain ε_t, Eq. (4.54) represents that by providing lateral confinement the concrete stress f_c increases 1.93 times the confining stress by CFS at ε_t. In the same way, the term of 2.2 $\rho_s f_{yh}$ in the right hand side of Eq. (4.62) (circular sections) represents an increasing rate of the concrete stress f_c at $\varepsilon_c = \varepsilon_t$ by providing confinement by ties.

Consequently, the increasing rate of concrete stress f_t by CFS and that by ties may be added if a concrete cylinder is confined by both CFS and ties. If this assumption is valid, the stress f_t of a concrete cylinder which is confined by both CFS and ties may be written from Eqs. (4.54), (4.57), and (4.62) as

$$\frac{f_t}{f_{c0}} = \begin{cases} 1.0 + 1.93 \dfrac{\rho_{CF} \varepsilon_{CF} E_{CF}}{f_{c0}} + 2.2 \dfrac{\rho_s f_{yh}}{f_{c0}} & \text{circular sections} \\ 1.0 + 1.53 \dfrac{\rho_{CF} \varepsilon_{CF} E_{CF}}{f_{c0}} + 0.76 \dfrac{\rho_s f_{yh}}{f_{c0}} & \text{square sections} \end{cases} \tag{4.65}$$

In a similar way, the strain ε_t corresponding to f_t may be written as

$$\varepsilon_t = \begin{cases} 0.003 + 0.00939 \dfrac{\rho_{CF} \varepsilon_{CF} E_{CF}}{f_{c0}} + 0.0107 \dfrac{\rho_s f_{yh}}{f_{c0}} & \text{circular sections} \\ 0.003 + 0.0095 \dfrac{\rho_{\mathrm{CF}} \varepsilon_{CF} E_{CF}}{f_{c0}} + 0.0114 \dfrac{\rho_s f_{yh}}{f_{c0}} & \text{square sections} \end{cases} \tag{4.66}$$

On the other hand, in Eqs. (4.46) and (4.47) the denominator in the first term of the right hand side ($\rho_{CF} \varepsilon_{CF} E_{CF}$) represents the confining stress of CFS at the strain ε_{CFt}. Similarly, $\rho_s f_{yh}$ in the denominator in Eq. (4.64) represents the confining stress by ties at the strain ε_{CFt}. It is noted that concrete start to remarkably deteriorate when the concrete strain in the spherical direction reaches ε_{CFt} ($\approx$1,500-1,900 μ), and this is close to the yield strain of ties ε_{yh} ($\approx$1,800 μ). As a consequence, denoting E_s the elastic modulus of ties, $\rho_s f_{yh}$ in Eq. (4.64) may be written as

$$\rho_s f_{yh} = \rho_s \varepsilon_{yh} E_s \approx \rho_s \varepsilon_{CFt} E_s \tag{4.67}$$

Based on this assumption, the confining stress by CFS represented by Eqs. (4.46) and (4.47) and the confining stress by ties represented by Eq. (4.63) may be added to obtain the confining stress of concrete confined by both CFS and ties.

On the other hand, the second term of Eq. (4.63) represents a rate of continuous increase of concrete stress at strains over ε_{CFt}. Since the confining stress of ties does not any more increase after their yield, this confining stress by ties is not needed to add to the second term of q. (4.63). Consequently, E_g of a concrete cylinder confined by both CFS and ties may be written from Eqs. (4.46), (4.47) and (4.63) as

$$E_g = \begin{cases} -0.658 \dfrac{f_{c0}{}^2}{\rho_{CF} \varepsilon_{CFt} E_{CF} + 0.098 \rho_s f_{yh}} + 0.078 \sqrt{\rho_{CF}} E_{CF} & \text{circular sections} \\ -1.198 \dfrac{f_{c0}{}^2}{\rho_{Cf} \varepsilon_{CFt} E_{CF} + 0.107 \rho_s f_{yh}} + 0.012 \sqrt{\rho_{CF}} E_{CF} & \text{square sections} \end{cases} \tag{4.68}$$

Since a concrete cylinder confined by both CFS and ties reaches its ultimate when CFS ruptures, Eqs. (4.56) and (4.59) still provide the ultimate strain.

To verify the empirical constitutive model by Eqs. (4.65), (4.66), (4.68), (4.56), and (4.59), loading tests were conducted for concrete cylinders with various confinement by CFS and ties.

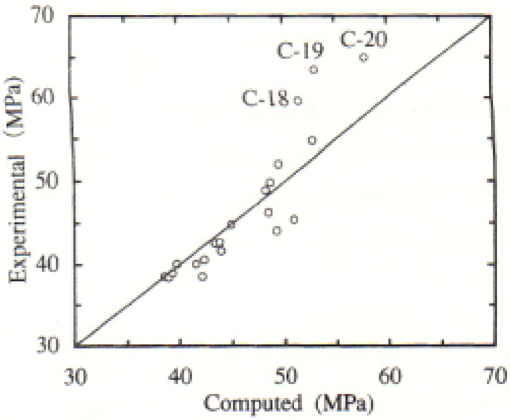

(a) f_t

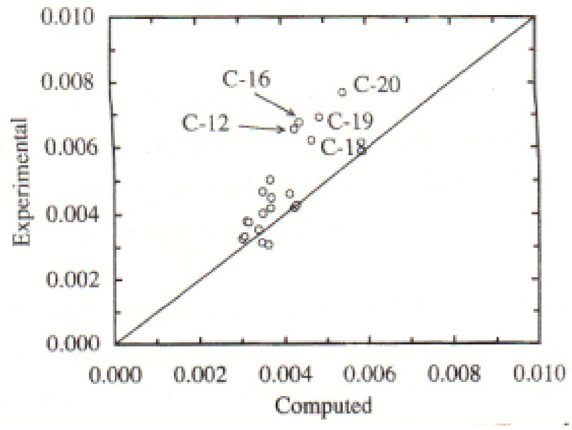

(b) ε_t

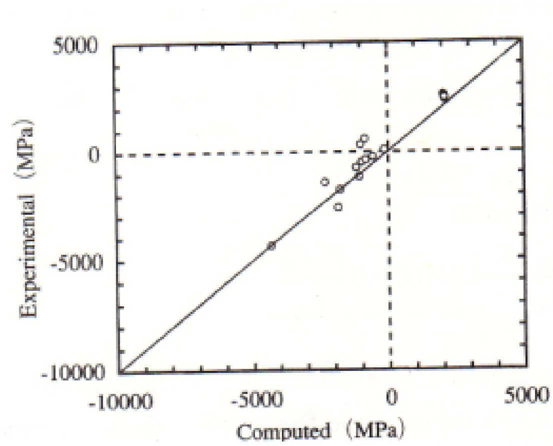

(c) E_g

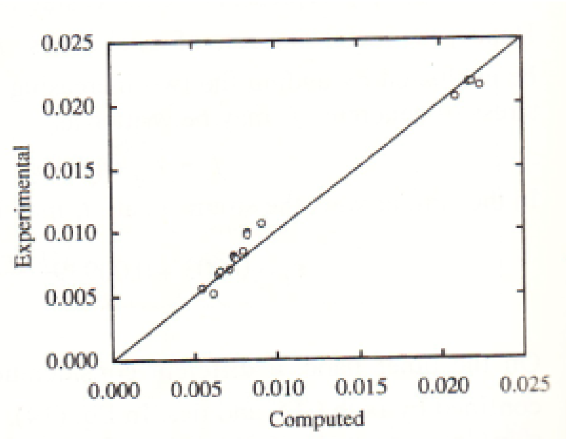

(d) ε_{cu}

Fig.4.12 Comparison of Empirical Parameters and Experimental Results

Fig. 4.12 shows the validation of empirical evaluation of f_t, ε_t, E_g and ε_{cu}. The empirical parameters well agree with the experimental results. Using those parameters stress vs. strain relations of concrete confined by various amount of CFS and ties are evaluated to compare with the experimental results. Fig. 4.13 shows an example of the comparison. The empirical stress vs. strain relations agree well with the experimental results.

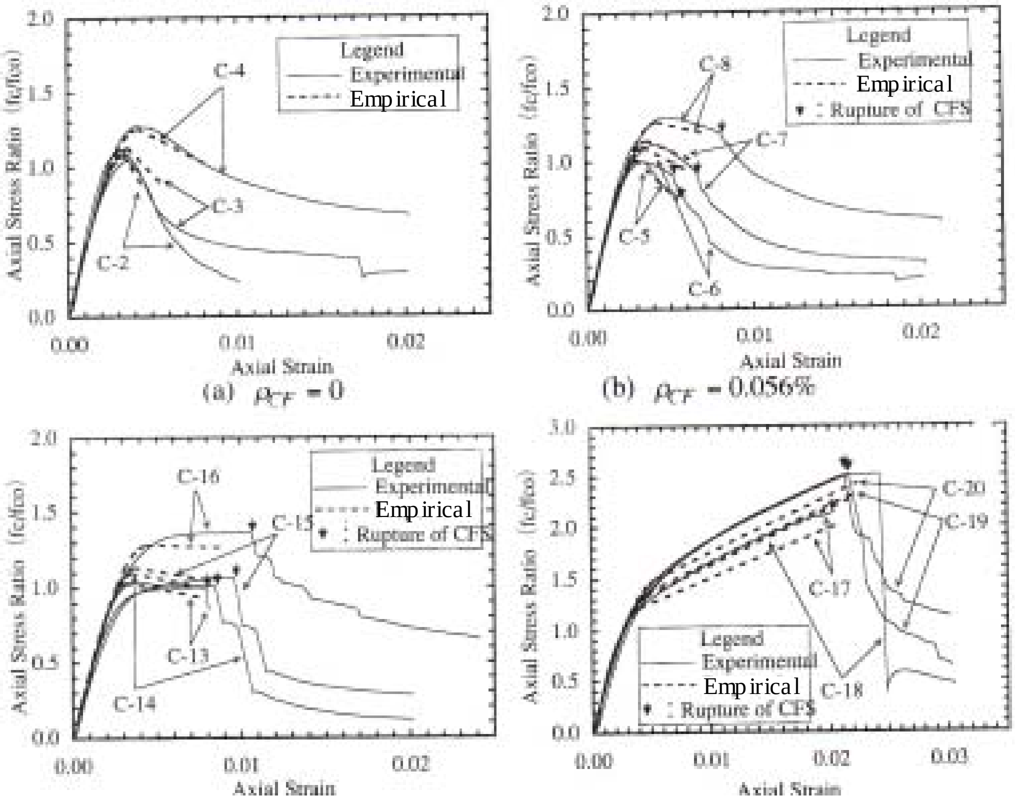

Fig.4.13 Empirical and Experimental Stress vs. Strain Relations of Concrete Confined by CFS and Ties